Associated photoproduction of K^+ mesons off protons within a coupled-channels K-matrix approach

R. Shyam,[1,2,*] O. Scholten,[3] and H. Lenske[1]
[1]*Institute für Theoretische Physik, Universität Giessen, D-35392 Giessen, Germany*
[2]*Saha Institute of Nuclear Physics, Kolkata 70064, India*
[3]*Kernfysisch Versneller Instituut, University of Groningen, NL-9747 AA Groningen, The Netherlands*
(Received 19 November 2009; published 14 January 2010)

We investigate the $p(\gamma,K^+)\Lambda$ and $p(\gamma,K^+)\Sigma^0$ reactions within a coupled-channels effective-Lagrangian method that is based on the K-matrix approach. The two-body final channels included are πN, ηN, ϕN, ρN, γN, $K\Lambda$, and $K\Sigma$. Nonresonant meson-baryon interactions are included in the model via nucleon intermediate states in the s and u channels and meson exchanges in the t-channel amplitude and the u-channel resonances. The nucleon resonances $S_{11}(1535)$, $S_{11}(1650)$, $S_{31}(1620)$, $P_{11}(1440)$, $P_{11}(1710)$, $P_{13}(1720)$, $P_{33}(1232)$, $P_{33}(1600)$, $D_{13}(1520)$, $D_{13}(1700)$, and $D_{33}(1700)$ are included explicitly in the calculations. With a single parameter set that was derived earlier from our analysis of η-meson photoproduction, the model describes all the available cross-section and polarization data of the SAPHIR Collaboration well for the two investigated channels. The description of the data from the CLAS Collaboration, however, is not of the same quality. In contrast to some previous studies, we do not find any compelling need to include a D_{13} state with a mass of about 2.0 GeV to reproduce the data for the $p(\gamma,K^+)\Lambda$ reaction at photon energies corresponding to the invariant mass around 1.9 GeV.

DOI: 10.1103/PhysRevC.81.015204 PACS number(s): 13.60.Le, 13.75.Cs, 11.80.−m, 12.40.Vv

I. INTRODUCTION

Recently, several laboratories have devoted a considerable amount of effort to the investigation of the photoproduction of strangeness on the nucleon. Experiments performed at JLab-CLAS [1,2], ELSA-SAPHIR [3,4], and SPring8/LEPS [5,6] have produced high-quality data on the associate strangeness production reactions $p(\gamma,K^+)\Lambda$ and $p(\gamma,K^+)\Sigma^0$ covering the photon energy regime from threshold up to 3.0 GeV. Furthermore, data on single and double polarization [7] observables have also become available. The motivation behind these studies has been the fact that a considerable part of the excitation spectrum of the nucleon can, in principle, participate in the production process of associated strangeness ($K^+\Lambda$ and $K^+\Sigma^0$) through these reactions, because even at the threshold they involve invariant masses that exceed those of several baryonic resonances. It is hoped that these studies will help in investigating the so-called missing baryonic resonances that are predicted by the quark models (see, e.g., Ref. [8]) but not observed in nonstrange meson photoproduction. Some of these resonances may couple strongly to the $K\Lambda$ and $K\Sigma$ channels.

Determination of the properties of the nucleon resonances (e.g., their masses, widths, and coupling constants to various decay channels) is an important issue in hadron physics. This will help in testing the predictions of lattice quantum chromodynamics (LQCD), which is the only theory that tries to calculate these properties from first principles. Even though the computational power required for their numerical realization is enormous, such calculations have started to provide results for the properties of nucleon ground as well as excited states [9–13]. Furthermore, reliable nucleon resonance data are important for testing the "quantum-chromodynamics (QCD)-based" quark models of the nucleon (see, e.g., Refs. [8] and [14]) and also the dynamical coupled-channels models of baryonic resonances [15].

One of the major challenges in this field is the extraction of reliable information about nucleon resonance properties from the photoproduction data. In experiments, these resonances are excited as intermediate states before decaying into the final meson and baryon channels. A good description of intermediate-energy scattering is still not amenable to the LQCD calculations. Therefore, at this stage the effective methods are usually employed to describe the dynamics of the meson production reactions. Baryon resonance states are included explicitly in these approaches and their properties are obtained by comparing the predictions of the theory with the experimental data [16–21].

To determine resonance properties reliably from the experimental measurements, a model is required that can analyze the different reactions over the entire energy range using a single Lagrangian density that generates all nonresonance contributions from Born, u-channel, and t-channel contributions without introducing new parameters. At the same time, the Lagrangian should also satisfy the symmetries of the fundamental theory (i.e., QCD) while retaining only mesons and baryons as effective degrees of freedom.

The coupled-channels method within the K-matrix approach [22–28] provides a way to analyze simultaneously all reaction data for a multitude of observables in different reaction channels while respecting the constraints described above. This method is attractive because it is based on an effective-Lagrangian framework that is gauge invariant and is consistent with chiral symmetry. It also provides a convenient way of imposing the unitarity constraint. This results from the Bethe-Saltpeter equation in the approximation where particles forming the loop are taken on the mass shell, that is, only the

*shyam@theory.saha.ernet.in

discontinuity part of the loop integral is retained. The S matrix in this approach is unitary provided that the K matrix is taken to be real and Hermitian.

Alternatively, the dynamical coupled-channels models within the Hamiltonian formalism have also been used to describe meson production reactions [29–35]. Isobaric models such as Kaon-Maid [36] and Saclay-Lyon [37] were utilized in Refs. [38] and [39] to describe the $p(\gamma, K^+)\Lambda$ reaction. This reaction has also been studied within a variety of tree-level isobar models [40–43] and in quark models [44–46]. In Ref. [47] a gauge-invariant chiral unitary framework is used to describe the photoproduction data of both the SAPHIR and the CLAS Collaborations.

The main objective of this paper is to study the photoproduction reactions $p(\gamma, K^+)\Lambda$ and $p(\gamma, K^+)\Sigma^0$ for photon energies ranging from threshold to about 3 GeV in a coupled-channels formalism from Refs. [25], [27], and [28] that is based on the K-matrix approach. This is an effective-Lagrangian model that is gauge invariant and obeys the low-energy theorem. We aim to describe simultaneously the data on total and differential cross sections (DCSs) as well as on polarization observables for both the reactions within the same framework with a single parameter set. The Λ and Σ^0 hyperons have isospins of 0 and 1, respectively. Thus, the intermediate states of $K^+\Lambda$ have isospin $\frac{1}{2}$ only (N^*), whereas those of $K^+\Sigma^0$ can have both $\frac{1}{2}$ and $\frac{3}{2}$ isospins (N^* and Δ). Therefore, a combined description of all the available data for both these channels is indeed quite interesting and is a challenge to any theoretical model.

We would like to add that a subset of SAPHIR and CLAS data for the $p(\gamma, K^+)\Lambda$ reaction has been investigated previously, in Ref. [26], within the Giessen model, which is also a coupled-channels effective-Lagrangian K-matrix approach. Despite some differences in details (see the discussions in Ref. [28]), our method is similar to that of the Giessen model. The calculations presented in Ref. [26] have reproduced the $p(\gamma, K^+)\Lambda$ data well, with a slight preference for the SAPHIR data. In the present work we have attempted to describe the $p(\gamma, K^+)\Sigma^0$ reaction along with the $p(\gamma, K^+)\Lambda$ one within the same framework using the same parameter set, which already makes our analysis self-contained. Nevertheless, by comparing our results with those of the Giessen model, we expect to gain further insight into the mechanism of the strangeness photoproduction off proton.

Our paper is organized as follows. An overview of our model is given in Sec. II. This consists of a short discussion of the K-matrix formalism, the model space, and the channels included, the Lagrangians, and the form factors. Our results and their discussion are presented in Sec. III. A summary and conclusions of our work are presented in Sec. IV. Finally, forms of Lagrangians at various vertices are given in the Appendix.

II. DESCRIPTION OF THE MODEL

This work is based on an effective-Lagrangian model. The kernel in the K-matrix approach is built by using the effective Lagrangian as given in the Appendix. We have taken into account contributions from (i) the nucleon Born term, (ii) t-channel exchanges of mesons, (iii) nucleon and resonance terms in the u channel, and (iv) baryonic resonance in the s channel (see Fig. 1). The sum of amplitudes (i), (ii), and (iii) is termed the background contribution. As discussed here, this approach allows us to account for coupled-channels effects while preserving many symmetries of a full field-theoretical method.

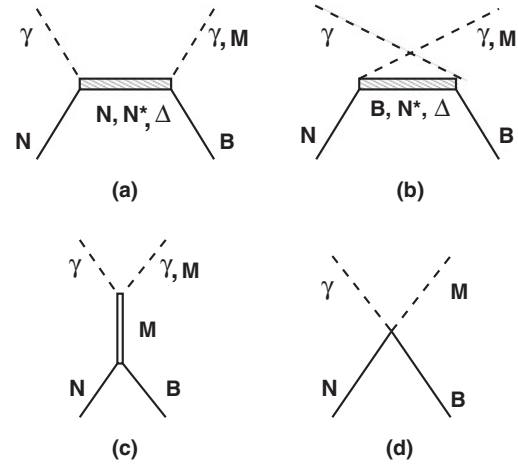

FIG. 1. (Color online) Feynman diagrams included in this work. (a, b) s- and u-channel diagrams with propagating final-state baryons ($B = N, \Lambda, \Sigma$) or intermediate-state resonances (Δ, N^*). M stands for mesons included in the model space. (c, d) t-channel contributions with propagating asymptotic and intermediate mesons, and the contact term required by the gauge invariance.

A. K-matrix model

The coupled-channels (or rescattering) effects are included in our model via the K-matrix formalism. In this section we present a short overview of this approach; a more detailed description is given in Refs. [23], [25], [48], and [49].

In the K-matrix formalism the scattering matrix is written as

$$\mathsf{T} = \frac{K}{1 - iK}. \tag{1}$$

It is easy to check that the resulting scattering amplitude $S = 1 + 2i\mathsf{T}$ is unitary provided that K is Hermitian. The construction in Eq. (1) can be regarded as the resummation of an infinite series of loop diagrams by making a series expansion,

$$\mathsf{T} = K + iKK + i^2KKK + \cdots. \tag{2}$$

The product of two K matrices can be rewritten as a sum of different one-loop contributions (three- and four-point vertex and self-energy corrections) depending on Feynman diagrams that are included in the kernel K. However, the entire spectrum of loop corrections present in a true field-theoretical approach is not generated in this way and the missing ones should be accounted for in the kernel. In constructing the kernel, care should be taken to avoid double counting. For this reason we include in the kernel tree-level diagrams only [Figs. 1(a)–1(c)],

modified with form factors and contact terms [Fig. 1(d)]. The contact terms (or four-point vertices) ensure gauge invariance of the model and express model dependence in working with form factors (see Sec. II C). Inclusion of both s- and u-channel diagrams [Figs 1(a) and 1(b), respectively] in the kernel ensures the compliance with crossing symmetry.

To be more specific, the loop corrections generated in the K-matrix procedure include only those diagrams that correspond to two on-mass-shell particles in the loop [50,51]. This is the minimal set of diagrams one has to include to ensure two-particle unitarity. Thus, any diagrams that are not two particle reducible (e.g., $\gamma N \to 2\pi N$ channels) are not included. In addition, only the convergent pole contributions, that is, the imaginary parts of the loop correction, are generated. The omitted real parts are important to guarantee analyticity of the amplitude and may have complicated cusplike structures at energies where other reaction channels open. In principle, these can be included as form factors as is done in the dressed K-matrix procedure [50,52]. We have chosen to work with purely phenomenological form factors for simplicity. An alternative procedure to account for the real-loop corrections is offered in Refs. [53–55].

The strength of the K-matrix procedure is that, despite its simplicity, several symmetries are obeyed by it [48]. As already noted, the resulting amplitude is unitary provided that K is Hermitian, and it obeys gauge invariance provided that the kernel is gauge invariant. In addition, the scattering amplitude complies with crossing symmetry when the kernel is crossing symmetric. This property is crucial for proper behavior of the scattering amplitude in the low-energy limit [51,56]. Coupled-channels effects are automatically accounted for by this approach for the channels explicitly included in the K matrix as the final states.

As a result of this channel coupling, the resonances generate widths that are compatible with their decays to channels included in the model space. For some resonances, such as Δ and $S_{11}(1535)$, this corresponds to their total width. Other resonances, particularly the high-lying ones, may have important decay branches to states that are not included in the model basis. To account for this in our calculations, we have added an explicit dissipative part to the corresponding propagators. The magnitudes of these widths are equivalent to decay widths of the resonances to states outside of our model space.

The resonances that are taken into account in building the kernel are summarized in Table I. In the current work we limit ourselves to the spin-$\frac{1}{2}$ and spin-$\frac{3}{2}$ resonances, as in this energy regime higher spin resonances are known [26] to give only a minor contribution to the $K^+\Lambda$ channel. Spin-$\frac{3}{2}$ resonances are included with so-called gauge-invariant vertices, which have the property that the coupling to spin-$\frac{1}{2}$ pieces in the Rarita-Schwinger propagator vanishes [50,57,58]. We have chosen this prescription because it reduces the number of parameters, as we do not have to deal with the off-shell couplings. The effects of these off-shell couplings can be absorbed in contact terms [58], which we prefer, certainly within the context of the present work.

The masses of the resonances given in Table I are bare masses and they thus may deviate from the values given by the Particle Data Group [59]. Higher-order effects in the K-matrix formalism do give rise to a (small) shift of the pole position with respect to the bare masses. The masses of very broad resonances, in particular, P_{11}, are not well determined: values lying in a broad range (typically a spread of the order of a quarter of the width) give comparable results. The width reported in Table I corresponds to the partial width for decay to states outside our model space. The parameters reported in Table I are mostly unchanged compared to those presented in previous calculations within this model [25,27,28]. The t-channel contributions that are included in the kernel are summarized in Table II.

TABLE I. Baryon states included in the calculation of the kernel, with their coupling constants. Column "WD" lists the decay width to states outside the model space. See text for a discussion of the signs of the coupling constants.

L_{IJ}	M (GeV)	WD (GeV)	$g_{N\pi}$	$g^1_{p\gamma}$	$g^2_{p\gamma}$	$g_{K\Lambda}$	$g_{K\Sigma}$	$g_{N\eta}$
$S_{11}(1535)$	1.525	0.0	0.6	−0.60	–	0.1	0.0	2.2
$S_{11}(1650)$	1.690	0.030	1.0	−0.45	–	−0.1	0.0	−0.8
$S_{31}(1620)$	1.630	0.100	3.7	−0.12	–	–	−0.8	–
$P_{11}(1440)$	1.520	0.200	5.5	0.65	–	0.0	−2.0	0.0
$P_{11}(1710)$	1.850	0.300	3.0	0.25	–	0.0	−3.0	2.0
$P_{13}(1720)$	1.750	0.300	0.12	−0.75	0.25	−0.05	0.0	0.12
$P_{33}(1230)$	1.230	0.0	1.7	−2.2	−2.7	–	0.0	–
$P_{33}(1600)$	1.855	0.150	0.0	−0.4	−0.6	–	0.55	–
$D_{13}(1520)$	1.515	0.050	1.2	2.6	2.5	2.0	0.0	1.2
$D_{13}(1700)$	1.700	0.090	0.0	−0.5	0.0	0.0	0.3	−0.04
$D_{33}(1700)$	1.670	0.250	0.8	1.5	0.6	–	−3.0	–

B. Model space and channels included

To keep the model manageable and relatively simple, we consider only stable particles or narrow resonances in two-body final states. ΛK, ΣK, $N\phi$, $N\eta$, and $N\gamma$ are the final states of primary interest, and the $N\pi$ final state is included for its strong coupling to most of the resonances. Three-body final states, such as $2\pi N$, are not included explicitly as stated

TABLE II. Mass, spin, parity, and isospin of the mesons included in the model. The rightmost column specifies in which reaction channels their t-channel contributions are taken into account.

Meson	M (GeV)	S^π	I	t-channel contributions
π	0.135	0^-	1	$(\gamma N \to \phi N)$, $(\pi N \to \rho N)$
K	0.494	0^-	$\frac{1}{2}$	$(\gamma N \to K\Lambda)$, $(\gamma N \to K\Sigma)$
ϕ	1.019	1^-	0	
η	0.547	0^-	0	$(\gamma N \to \phi N)$
ρ	0.770	1^-	1	$(\gamma N \to \pi N)$, $(\gamma N \to \eta N)$, $(K\Lambda \to K\Sigma)$, $(K\Sigma \to K\Sigma)$, $(N\pi \to K\Lambda)$, $(N\pi \to N\eta)$, $(N\pi \to N\pi)$
ω	0.781	1^-	0	$(N\gamma \to N\pi)$, $(N\gamma \to N\eta)$
σ	0.760	0^+	0	$(N\gamma \to N\phi)$, $(N\pi \to N\pi)$
K^*	0.892	1^-	$\frac{1}{2}$	$(N\gamma \to K\Lambda)$, $(N\gamma \to K\Sigma)$, $(K\Lambda \to N\eta)$, $(K\Sigma \to N\eta)$, $(N\pi \to K\Sigma)$

above. Their influence on widths of resonances is taken into account by assigning an additional (energy dependent) width to them [23]. To investigate the effects of coupling to more complicated states, we have also included the $N\rho$ final state. As shown in Ref. [25], inclusion of the ρ channel has a strong influence on the pion sector but only a relatively minor effect on Λ and Σ photoproduction.

The components of the kernel that couple the different nonelectromagnetic channels are taken as the sum of tree-level diagrams, similar to what is used for the photon channels. For these other channels no additional parameters were introduced and they thus need no further discussion.

C. Form factors and gauge restoration

Without the introduction of form factors, calculations with Born terms strongly overestimate the cross section at higher energies. Although inclusion of coupled-channels effects reduces the cross section at high energies, disagreement with the experimental data persists. Therefore, the Born contribution will have to be quenched with form factors. There are two physical motivations for introducing form factors (or vertex functions). The first is that, at high photon energies, one may expect sensitivity to the short-range quark structure of the nucleon. Because this physics is not included explicitly in our model, we can only account for it through the introduction of phenomenological vertex functions. The second reason has to do with the intermediate-range effects caused by meson-loop corrections that are not generated through the K-matrix formalism. Examples of these are given in Refs. [50] and [52].

In our approach as well as that in Ref. [24], the form factors are not known *a priori* and thus they introduce a certain arbitrariness to the model. In the current paper we limit ourselves to dipole form factors in the s, u, and t channels because of their simplicity:

$$F_m(s) = \frac{\lambda^2}{\lambda^2 + (s - m^2)^2}, \tag{3}$$

where m is the mass of the propagating particle and λ is the cutoff parameter. For ease of notation we introduce the subtracted form factors

$$\tilde{f}_m(s) = \frac{1 - F_m(s)}{s - m^2}, \tag{4}$$

where $F_m(s)$ is normalized to unity on the mass shell, $F_m(m^2) = 1$, and $\tilde{f}_m(m^2)$ is finite.

However, in the kaon sector only, we use a different functional form for the u-channel form factors:

$$H_m(u) = \frac{u\lambda^2}{[\lambda^2 + (u - m^2)^2]m^2}. \tag{5}$$

The argumentation for this different choice is presented in the discussion of the Σ-photoproduction results in Ref. [25]. Often a different functional form and cutoff values are introduced for the t-channel form factors. Although this can easily be motivated, it introduces additional model dependence and increases the number of free parameters. To limit the overall number of parameters we have taken the same cutoff value [$\lambda = 1.2$ GeV^2; see Eq. (3)] for all form factors except for the Born contributions in kaon channels, where we used $\lambda = 1.0$ GeV^2.

Inclusion of form factors will in general break electromagnetic gauge invariance of the model. Therefore, a gauge-restoration procedure should be applied. In Ref. [25], the implications of various gauge-restoration procedures was studied for the $\gamma p \to K\Sigma$ amplitude. It was observed that the gauge-invariance restoration procedure is model dependent, which may give rise to strongly different Born contributions to the amplitude. Therefore, the choice of the procedure to be adopted is guided by its ability to describe the experimental data. It was found that the gauge-restoration procedure of Davidson and Workman [60] provided the best description of the data on $K\Sigma$ photoproduction. We have used this procedure in the present work also.

We note that fitting the pion scattering and pion photoproduction amplitudes fixes masses as well as pion and photon coupling constants for most of the resonances. This strongly limits the number of free parameters for the kaon production channels.

III. RESULTS AND DISCUSSION

Our aim in this paper is to use the database on $p(\gamma, K^+)\Lambda$ and $p(\gamma, K^+)\Sigma^0$ reactions from both the SAPHIR and the CLAS collaborations to check various ingredients of our unitary coupled-channels field-theoretic model of meson production in photon-induced reactions on nucleons. In particular, we are interested in checking to what extent a simultaneous fit to data for a multitude of observables for both the reactions can be obtained with a single set of input parameters. This is expected to provide a strong constraint on the model parameters, thus reducing the model dependence to a minimum. It is also likely to highlight the role of channel couplings in various regions of photon energies because several calculations of the associated kaon production reactions have neglected these effects.

We emphasize, however, that even the large experimental database may not allow us to fix the extracted parameters uniquely within the unitary coupled-channels effective-Lagrangian model [24]. This is because it is necessary to include empirical form factors in the model to regularize the amplitudes at higher energies. As mentioned before these form factors require a gauge-invariance restoration procedure that involves ambiguities. Nevertheless, confronting the model with a large database in several reaction channels is expected to provide a means to overcome this problem.

The parameters in the model have been adjusted [27] to reproduce the Virginia Tech partial wave amplitudes of Arndt *et al.* [61]. In Ref. [28] we presented a comparison of our calculated S-, P-, and D-wave amplitudes for pion-nucleon scattering for isospins $I = \frac{1}{2}$ and $\frac{3}{2}$ channels with those of the FA08 single-energy partial wave amplitudes in Ref. [61]. The corresponding results for pion photoproduction and Compton scattering are given in Ref. [27]. There we noted that both the real and the imaginary parts of the pion-nucleon scattering amplitudes are described well, although some differences start to show up at the upper limit of the energy range considered.

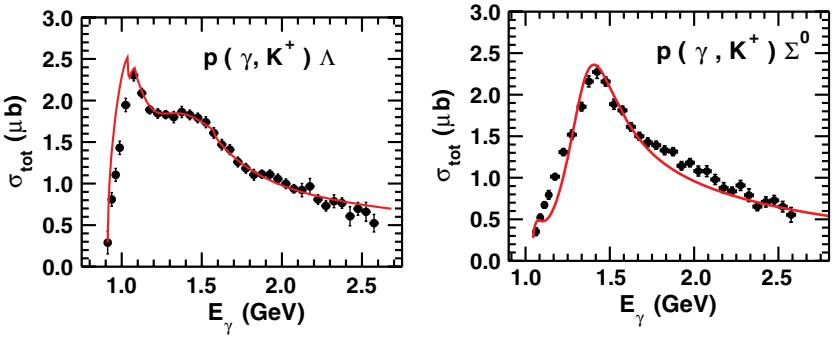

FIG. 2. (Color online) Comparison of the calculated total cross sections for the $p(\gamma,K^+)\Lambda$ and $p(\gamma,K^+)\Sigma^0$ reactions with the corresponding experimental data taken from Ref. [3].

The data for $p(\gamma,K^+)\Lambda$ and $p(\gamma,K^+)\Sigma^0$ reactions consist of total and DCSs and hyperon polarizations measured at CB-ELSA (SAPHIR Collaboration [3]) and at JLab (CLAS Collaboration [1,2]) for photon energies ranging from respective thresholds to about 3 GeV. Moreover, beam asymmetry data are available from the SPring8/LEPS [5,6] group for nine photon energy beams between 1.5 and 2.4 GeV. These data, therefore, cover not only the entire resonance region but also the region where the background contributions are expected to be dominant.

In Fig. 2, we compare the results of our calculations for the total cross sections with the corresponding data from the SAPHIR Collaboration [3] for $p(\gamma,K^+)\Lambda$ and $p(\gamma,K^+)\Sigma^0$ reactions. Photon energies (E_γ) range from threshold to about 2.6 GeV. The experimental cross sections for the $p(\gamma,K^+)\Lambda$ reaction show a steep rise as E_γ increases from threshold to about 1.1 GeV The latter corresponds to a γp-channel total invariant mass (W) of ≈1.7 GeV, which coincides with the masses of the $S_{11}(1650)$, $P_{11}(1710)$, and $P_{13}(1720)$ resonances. The decrease in the cross sections just before the threshold for the $K^+\Sigma^0$ channel indicates a cusp owing to the opening of this channel, which has been indicated in Refs. [25,62]. The data in this region are well reproduced by our calculations. There is also a second peak in the data, at $E_\gamma \approx 1.5$ GeV ($W \approx 1.9$ GeV). Our calculations also describe the data in this region well.

In contrast to studies reported in Refs. [21,38,39,63], we do not require an additional baryonic resonance $D_{13}(1895)$ to explain the data in the second peak region. Looking at the cross sections for the $p(\gamma,K^+)\Sigma^0$ reaction in Fig. 2 (right panel), one notices that the second maximum in the $p(\gamma,K^+)\Lambda$ data is centered around the same value of W where the only peak is observed in the $K^+\Sigma^0$ channel. Hence, peaks in the $p(\gamma,K^+)\Lambda$ total cross section are more likely to be the consequences of unitarity and multichannel dynamics. This is further supported by the coupled-channels analysis of this reaction reported in Ref. [26], where the second peak in the $K^+\Lambda$ total cross-section data is explained as resulting from the interference between background and resonance contributions and not from the presence of a $D_{13}(1895)$ resonant state. The same conclusion was also drawn in previous coupled-channels studies [24].

On the other hand, the total cross sections of the $p(\gamma,K^+)\Sigma^0$ reaction rise smoothly from threshold to its peak at $E_\gamma \approx 1.45$ GeV ($W \approx 1.9$ GeV). The cross sections drop smoothly for E_γ larger than this value. Our calculations are able to reproduce the data well in the entire region of photon energies with the exception of some far lower and some higher photon energies, where the data are somewhat underestimated.

In Fig. 3, we show the contribution of various resonances and background terms to the total cross sections of the $p(\gamma,K^+)\Lambda$ and $p(\gamma,K^+)\Sigma^0$ reactions as a function of E_γ. It is clear from this figure that whereas the background contributions dominate the $p(\gamma,K^+)\Lambda$ cross sections in the entire range of photon energies, they do so only for $E_\gamma >$ 1.5 GeV in the case of the $p(\gamma,K^+)\Sigma^0$ reaction. It is interesting

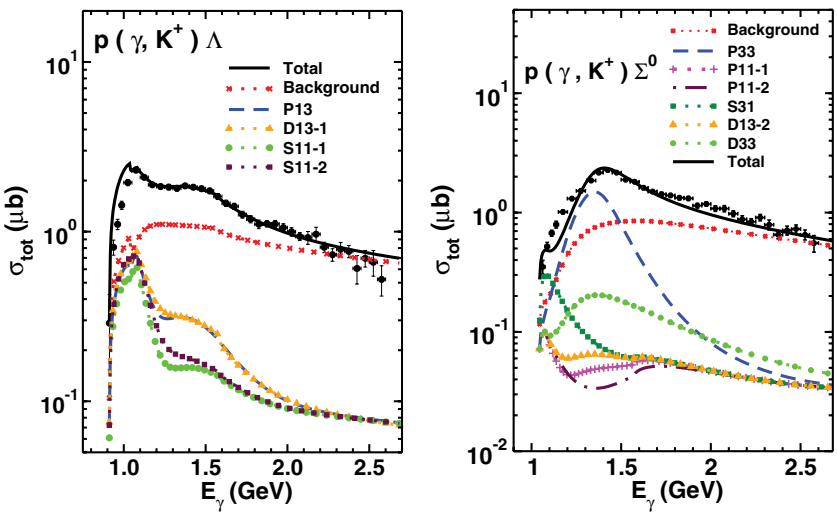

FIG. 3. (Color online) Partial wave decomposition of the calculated total cross sections for the same reactions as shown in Fig. 2. Contributions of different resonances are shown by various curves as indicated in the keys. Also shown are the background contributions, which consist of Born and u- and t-channel terms. Experimental data are taken from Ref. [3].

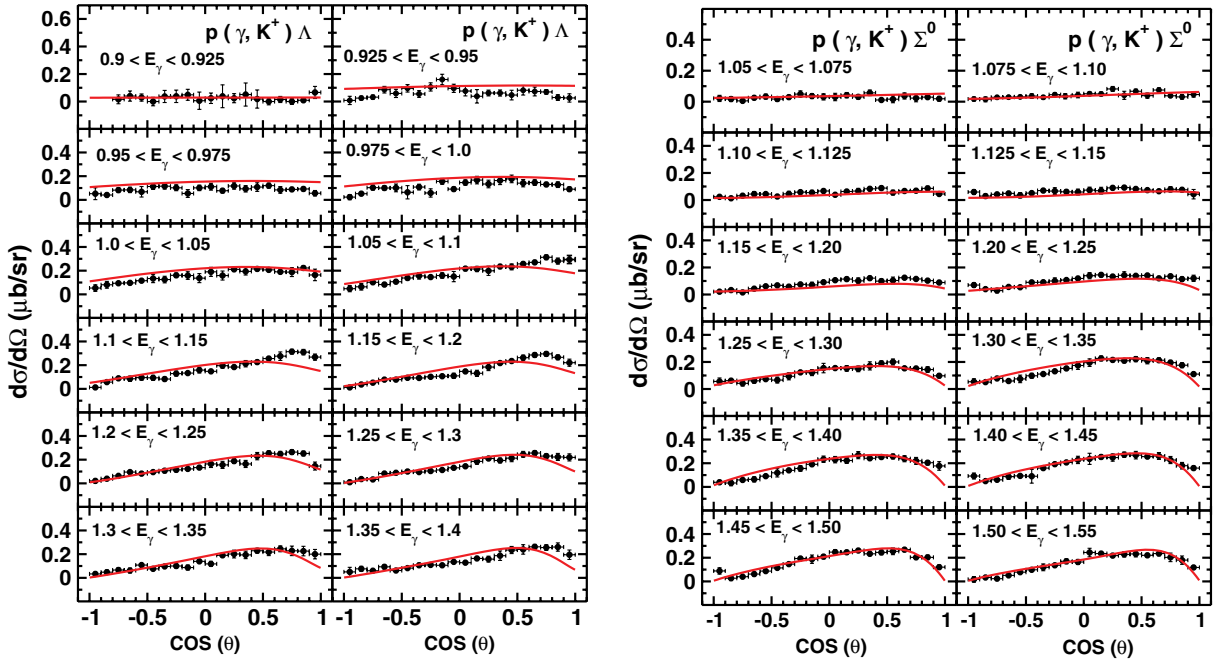

FIG. 4. (Color online) Comparison of the calculated and experimental differential cross sections for the $p(\gamma,K^+)\Lambda$ and $p(\gamma,K^+)\Sigma^0$ reactions as a function of the cosine of the K^+ c.m. angle for photon energies 0.94 GeV $< E_\gamma <$ 1.4 GeV and and 1.05 GeV $< E_\gamma <$ 1.55 GeV, respectively. The energy bin is indicated in each graph (as GeV). Experimental data are taken from Ref. [3].

to note that the contributions of the $P_{13}(1720)$, $S_{11}(1535)$, $S_{11}(1650)$, $P_{13}(1720)$, and $D_{13}(1520)$ resonances (depicted as $P13$, $S11$-1, $S11$-2, and $D13$-1, respectively, in the left panel in Fig. 3) peak at about the same value of E_γ ($\approx$1.1 GeV) in the $p(\gamma,K^+)\Lambda$ total cross section. In the region around this energy, the resonance contributions are comparable to those of the background terms, and they combine together to constitute the structure of the first peak in the data. Furthermore, no one resonance individually dominates in this region, which is in contrast to the results in Ref. [26]. The contributions of the $P_{11}(1710)$ resonance are very weak and are not included in our study. This is in agreement with the results in Ref. [26]. We have also excluded a third S_{11} resonance, with a mass and width of about 1.780 and 0.28 GeV, respectively, which was considered in descriptions of the $p(\gamma,\eta)p$ and $p(\gamma,K^+)\Lambda$ reactions in Refs. [33] and [46].

The peak region in the $p(\gamma,K^+)\Sigma^0$ total cross section, on the contrary, is dominated by the contributions from the spin-$\frac{3}{2}$, isospin-$\frac{3}{2}$ $P_{33}(1600)$ resonance. Apart from the background and, to a lesser extent, the $D_{33}(1700)$ terms, other resonances are almost unimportant in this region. Furthermore, the magnitudes of the $D_{13}(1700)$, $P_{11}(1440)$, and $P_{11}(1710)$ resonances (depicted as $D13$-2, $P11$-1, and $P11$-2, respectively, in the right panel in Fig. 3) are comparatively small over the entire range of photon energies. However, for E_γ very close to threshold the $S_{31}(1620)$ resonance is most important.

For both the reactions shown in Fig. 3, we note that the total cross sections beyond 2 GeV are almost solely governed by the contributions of the background terms. In this region all resonance contributions are small and comparable to each other.

DCSs provide more valuable information about the reaction mechanism. They reflect the quantum number of the excited state (baryonic resonance) when the cross section is dominated by it. DCSs include terms that weigh the interference terms of various components of the amplitude with the outgoing K^+ angles. Therefore, the structure of interference terms could highlight the contributions of different resonances in different angular regions. For the $p(\gamma,K^+)\Lambda$ and $p(\gamma,K^+)\Sigma^0$ reactions DCS data from the ELSA-SAPHIR group exist for 36 and 35 photon energy bins, respectively, in the range of respective thresholds to about 2.60 GeV covering a wide range of K^+ center-of-mass (c.m.) angles [3]. In the left panels in Figs. 4–6 we show comparisons of our calculations of DCSs with the corresponding SAPHIR data for the $p(\gamma,K^+)\Lambda$ reaction for energy bins in the range of 0.9–1.4, 1.4–2.0, and 2.0–2.6 GeV, respectively, whereas in the right panels the same are shown for the $p(\gamma,K^+)\Sigma^0$ reaction for photon energy bins in the range of 1.05–1.55, 1.55–2.15, and 2.15–2.55 GeV, respectively.

It is seen that the DCSs are flat as a function of kaon angle near the respective thresholds, which signifies the dominance of S-wave resonances near these energies. As E_γ increases further the DCSs develop a significant forward peaking, which is consistent with the domination of the background terms or the interference between background and s-channel resonance contributions. At still higher energies, the data show a tendency toward a slow rise at extreme forward angles.

It is clear that our model describes general trends of the data well in the complete photon energy regime of the SAPHIR measurement. However, a few specific details of the data are missed for some energy bins. In the regions of 1.0–1.20 and 1.45–1.8 GeV, the angular distributions at extreme

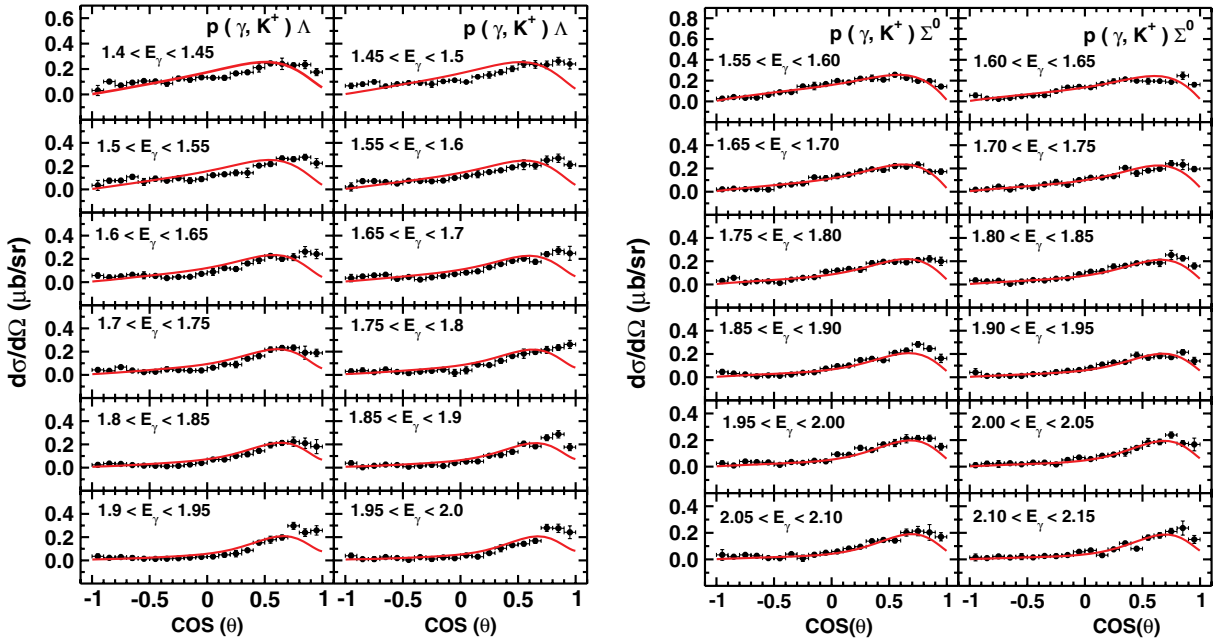

FIG. 5. (Color online) Same as Fig. 4 but for photon energies 1.4 GeV $< E_\gamma <$ 2.0 GeV and 1.55 GeV $< E_\gamma <$ 2.15 GeV, respectively. The energy bin is indicated in each graph (as GeV). Experimental data are taken from Ref. [3].

forward angles are not properly reproduced for the $p(\gamma, K^+)\Lambda$ reaction. However, those of the $p(\gamma, K^+)\Sigma^0$ reaction are well reproduced in these regions. At photon energies >2.0 GeV, the $p(\gamma, K^+)\Lambda$ cross sections show a tendency toward peaking at extreme forward angles, whereas the $p(\gamma, K^+)\Sigma^0$ data do not seem to do so. Within statistical errors our calculations are consistent with this trend of the data, although for the $K^+\Lambda$ channel the agreement is of a lesser quality compared to that for the $K^+\Sigma^0$ channel. In view of the fact that our background terms include both K and K^* exchange diagrams, with the same couplings for both reactions, we have obtained a reasonably good agreement with the data.

There are some discrepancies between the data from the ELSA-SAPHIR and those from the CLAS Collaboration. The CLAS group has reported consistently larger cross sections at most kaon angles for $E_\gamma > 1.19$ GeV. For certain

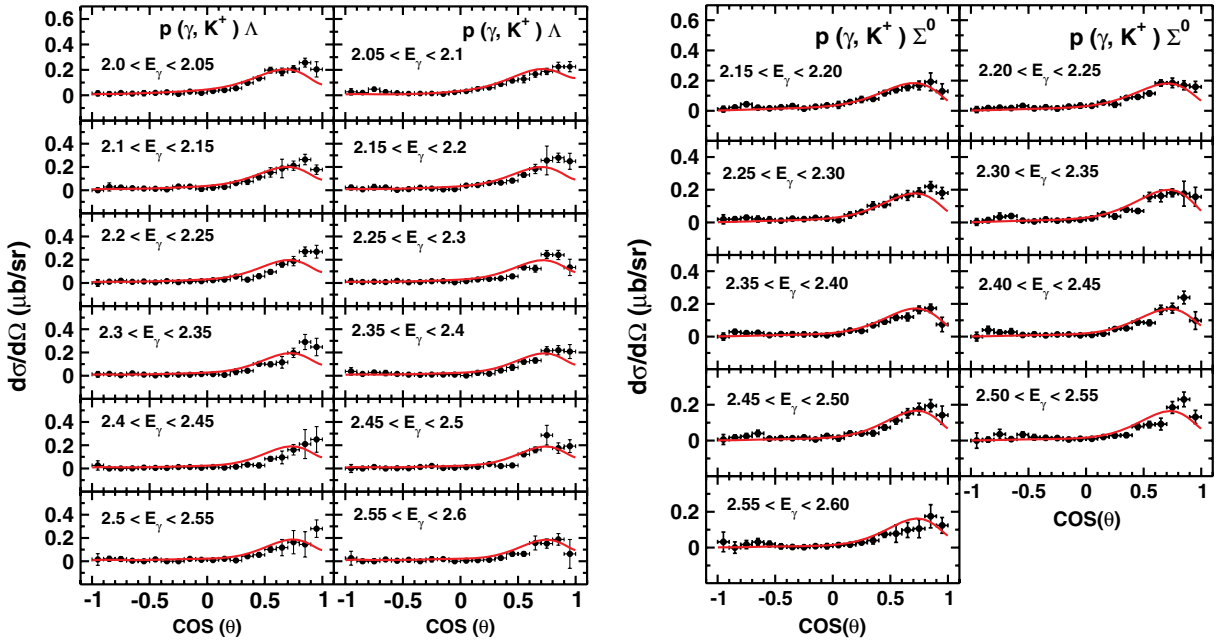

FIG. 6. (Color online) Same as Fig. 4 but for photon energies 2.0 GeV $< E_\gamma <$ 2.6 GeV and 2.15 GeV $< E_\gamma <$ 2.55 GeV, respectively. The energy bin is indicated in each graph (as GeV). Experimental data are taken from Ref. [3].

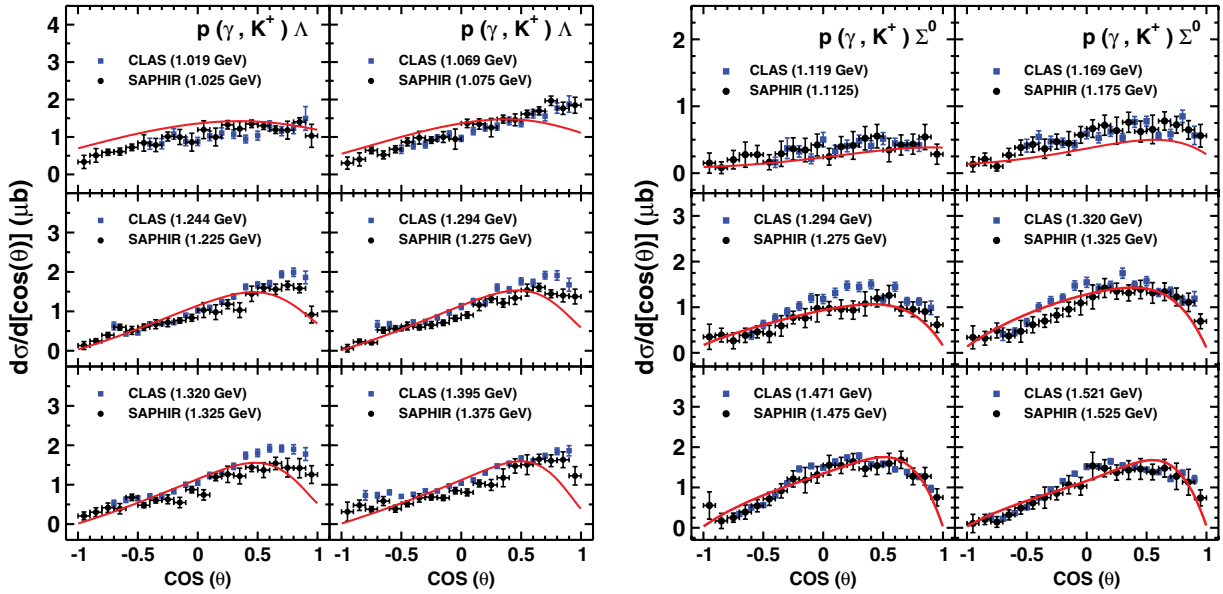

FIG. 7. (Color online) Comparison of calculated and experimental differential cross sections from the CLAS Collaboration [1] [filled (blue) squares] for the $p(\gamma,K^+)\Lambda$ and $p(\gamma,K^+)\Sigma^0$ reactions as a function of the cosine of the K^+ c.m. angle for selected bins of photon energy <1.5. Data from the SAPHIR Collaboration (taken from Ref. [3]) at nearby energies are also shown for comparison [filled (black) circles].

forward angles and photon energy bins one notices a large difference between the SAPHIR and the CLAS data for DCSs. Therefore, simultaneous description of the data from the two collaborations has often been problematic for theoretical models [34,39]. Our model is no exception. In Figs. 7 and 8, we show comparisons between our calculations and the CLAS data for DCSs for $p(\gamma,K^+)\Lambda$ and $p(\gamma,K^+)\Sigma^0$ reactions for 12 chosen photon energy bins. In these figures the SAPHIR data points are also given for comparison. Because the CLAS data are given in energy and angular bins different from those of the SAPHIR data, we have chosen those bins that are nearly equal in the two cases.

We note that the CLAS and SAPHIR data are identical for $E_\gamma < 1.1$ GeV for both reactions. However, at higher energies considerable differences are seen between the two data sets, particularly at forward angles. The CLAS DCS data for the $K^+\Lambda$ channel are more forward peaked for $E_\gamma \approx 1.2$–1.4 GeV compared to the SAPHIR data as well as our calculated cross sections. For the $K^+\Sigma^0$ case, the CLAS DCSs are consistently larger than the SAPHIR ones for all angles except the backward

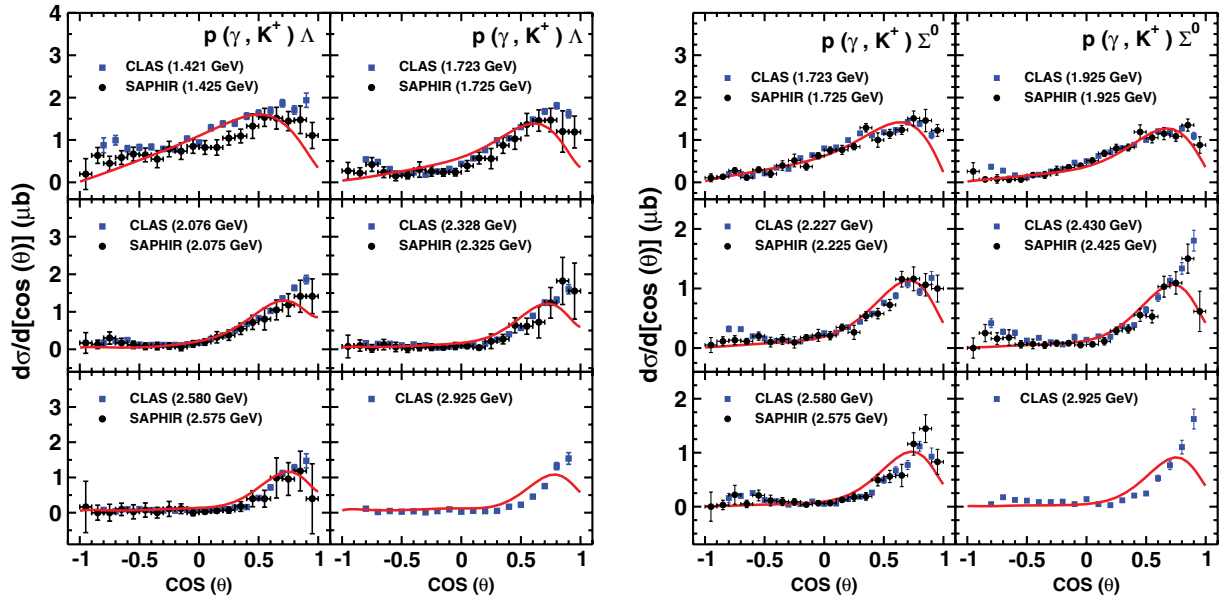

FIG. 8. (Color online) Same as Fig. 7 but for selected bins of photon energy >1.5 GeV.

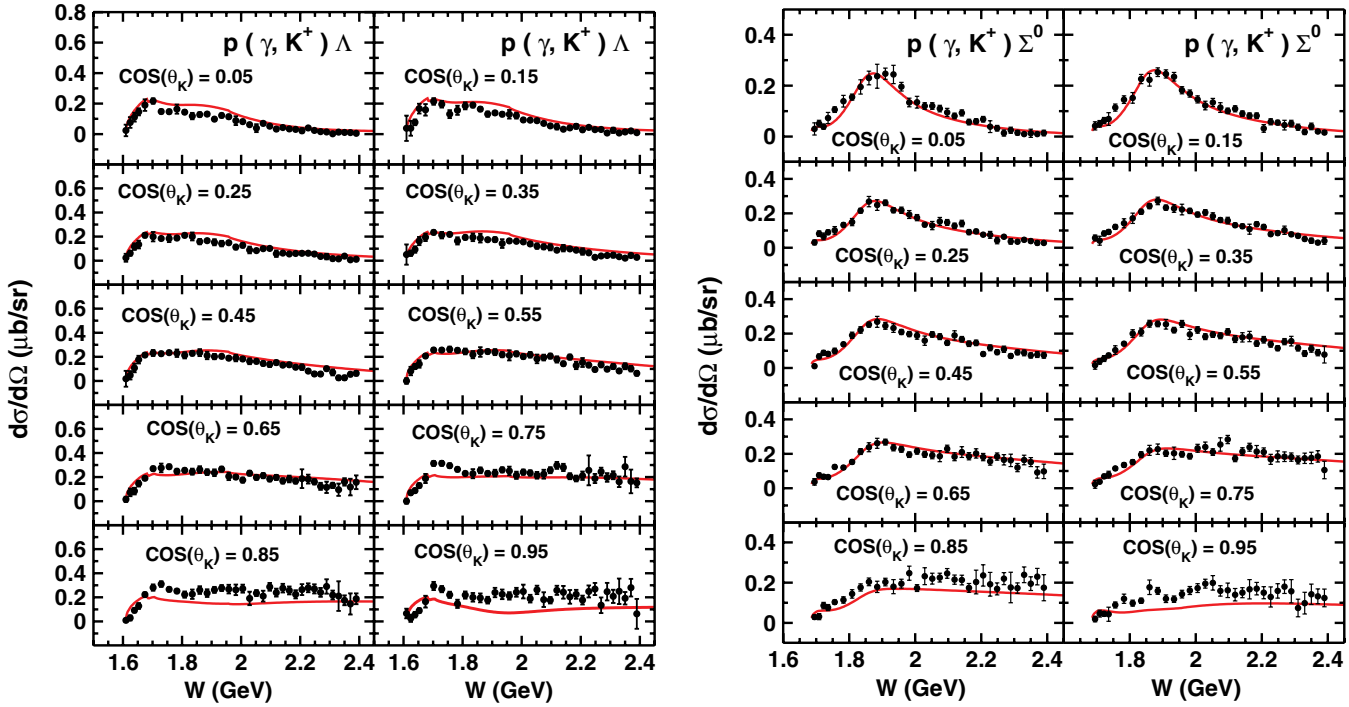

FIG. 9. (Color online) Comparison of calculated and experimental differential cross sections for the $p(\gamma,K^+)\Lambda$ and $p(\gamma,K^+)\Sigma^0$ reactions as a function of the γp invariant mass (W) for various positive cosines of the K^+ c.m. angle. Experimental data are taken from Ref. [3].

ones for E_γ between 1.25 and 1.5 GeV. Our calculations are unable to reproduce this feature.

For E_γ between 1.4 and 1.7 the $K^+\Lambda$-channel CLAS data have a tendency toward backward peaking as well, along with stronger forward peaking, which is again in contrast to the SAPHIR data as well as our calculations. The backward peaking of the CLAS data disappears for photon energies between 2.0 and 2.6 GeV, however, stronger forward peaking still remains and our calculations are unable to reproduce it fully. For the $p(\gamma,K^+)\Sigma^0$ reaction the CLAS data show some backward peaking at photon energies between 2.2 and 2.4 GeV. At other energies the differences between the data of the two groups are less noticeable for this channel. Our calculations are in better agreement with the CLAS data for these cases.

The resonance structure in the s channel should appear more clearly in the W dependence of the differential cross sections at various K^+ angles. In Fig. 9 (Fig. 10) we show the DCS for $p(\gamma,K^+)\Lambda$ and $p(\gamma,K^+)\Sigma^0$ reactions as a function of W for positive (negative) values of $\cos(\theta_{K^+})$. The experimental data are from the SAPHIR Collaboration. These figures show that the overall shapes of the W distributions are reproduced well by our calculations for all the angles for both reactions.

Nevertheless, we also note that, for the case of $K^+\Lambda$ production, our calculations underestimate the data somewhat for W between 1.7 and 2.0 GeV at forward angles [for $\cos(\theta_{K^+}) = 0.75$, 0.85, and 0.95]. As the bulk of the forward peaking is caused by t-channel exchanges, which are well understood, this leads to the suggestion that a contribution to the background is still missing. For the backward angles (see Fig. 9), the data on the $p(\gamma,K^+)\Lambda$ reaction show two peaks, at W around 1.7 and 1.9 GeV. Our calculations are able to reproduce the structure of both the peaks for all the angles except for the most backward one [$\cos(\theta_{K^+}) = 0.85$], where the peak at $W \approx 1.9$ GeV is underestimated. We would like to stress that, unlike Ref. [34], we find no need to include an additional D_{13} resonance (with mass ≈ 1.9 GeV and width $= 0.316$ GeV) to reproduce the data around 90^0. The underestimation of the peak for W around 1.9 GeV for $\cos(\theta_{K^+}) = 0.85$ might be seen as an indication of the need to include such a resonance. However, with the inclusion of this resonance the cross section increases for other backward angles also around this value of W [38] and the signs of the beam asymmetries turn out to be the opposite to what has been observed experimentally for this W [5].

On the other hand, for the $K^+\Sigma^0$ channel, the W dependence of the DCR (see Figs. 9 and 10) is reproduced very well by our calculations for all the angles [corresponding to both negative and positive values of $\cos(\theta_{K^+})$] with the exception of one very forward θ_{K^+}.

Polarization observables provide more sensitive tests of reaction models. The reason for this lies in the fact that these observables are generally very sensitive to the imaginary parts of the amplitudes, which are governed by coupling to other channels via the optical theorem. Data on hyperon recoil polarization (P_Y, with Y being Λ or Σ^0) have been reported by both the SAPHIR and the CLAS collaborations [2,3]. P_Y is related to interferences of the imaginary parts of the resonant amplitudes with real parts of other amplitudes including those of the background terms. In Fig. 11 we compare the results of our calculations of P_Y with the corresponding data from the SAPHIR Collaboration for $p(\gamma,K^+)\Lambda$ and $p(\gamma,K^+)\Sigma^0$

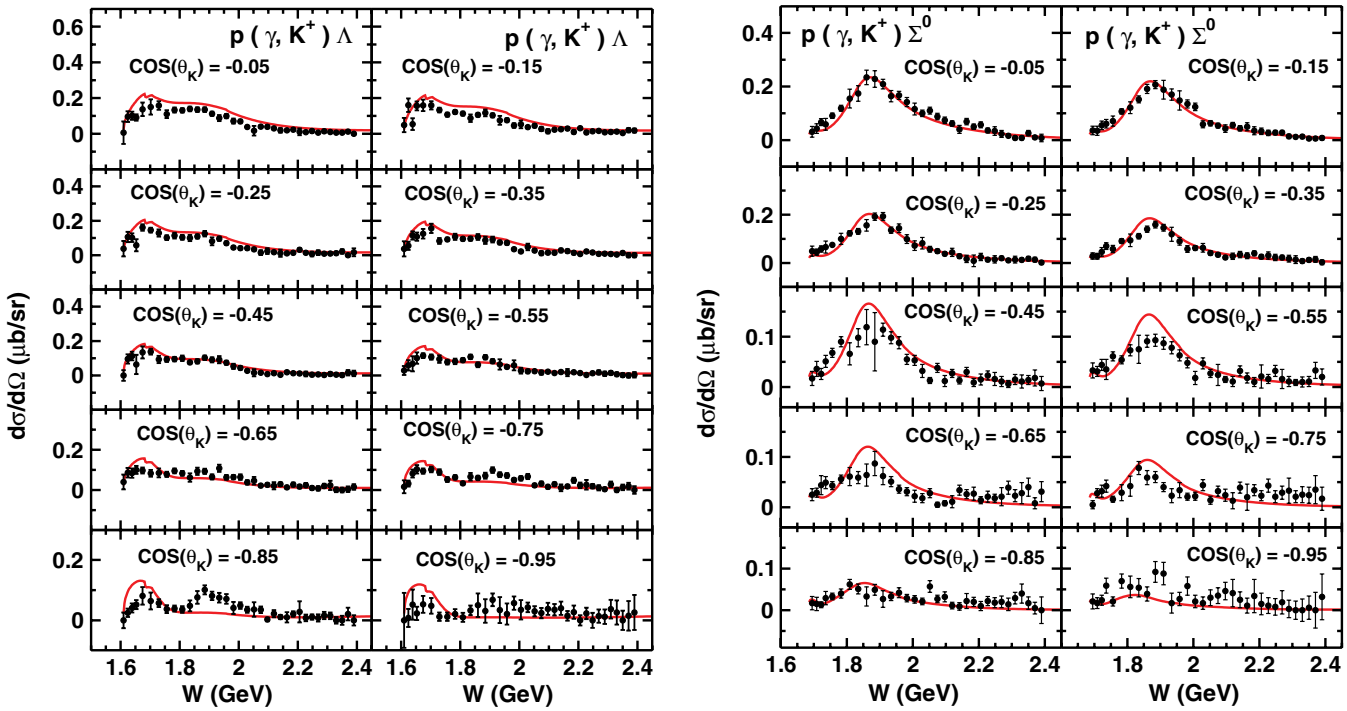

FIG. 10. (Color online) Same as Fig. 9 but for various negative cosines of the K^+ c.m. angle. Experimental data are taken from Ref. [3].

reactions. One notices that experimental P_Λ values tend to be positive at backward angles, nearly zero at angles around zero, and negative at forward angles. In contrast, P_{Σ^0} data show a nearly opposite trend. The CLAS P_Y data are used in the analyses in Refs. [34] and [38].

Our calculations reproduce approximately the trends seen in the data. The opposite signs of the observed P_Y of the two channels are nearly reproduced. The agreement with data is relatively better for E_γ below 1.6 GeV. The large positive back-angle polarizations seen in the P_Λ data are reproduced for all the photon energy bins. Similarly the large negative experimental P_{Σ^0} values at these angles are also nearly reproduced. At forward angles our model is relatively less successful in reproducing the P_Λ data at E_γ above 1.6 GeV. This again indicates perhaps some inadequacy of the background terms in our model.

Beam asymmetry (Σ_B) is the measure of the azimuthal anisotropy of a reaction yield relative to the linear polarization of the incoming photon. In Fig. 12 we compare the results of our calculations for this observable for both $p(\gamma,K^+)\Lambda$

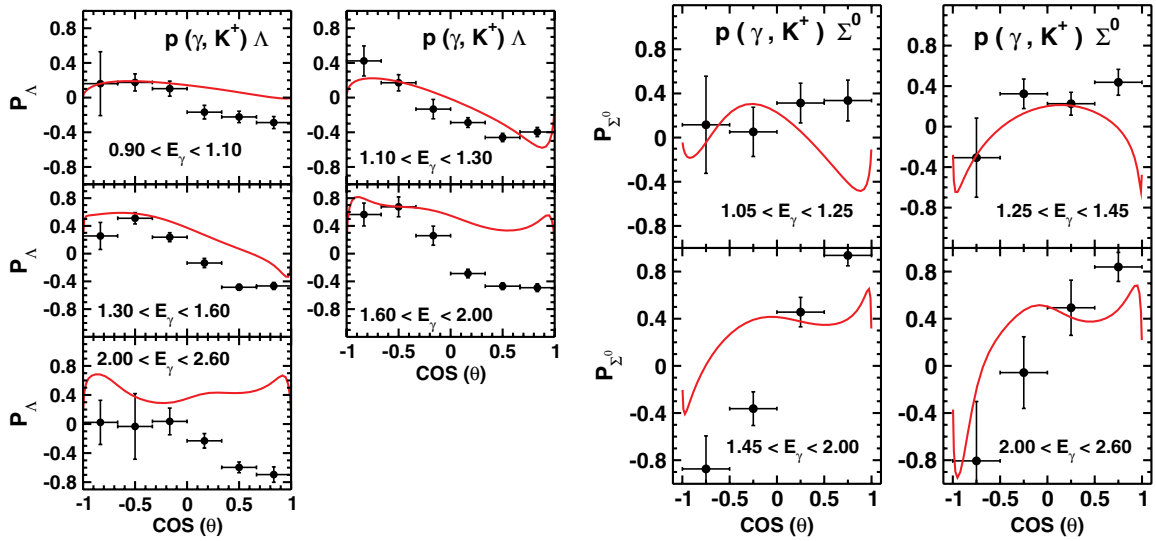

FIG. 11. (Color online) Comparison of our calculations with experimental data (taken from Ref. [3]) for hyperon polarization for the $p(\gamma,K^+)\Lambda$ and $p(\gamma,K^+)\Sigma^0$ reactions as a function of the cosine of the K^+ c.m. angle for the photon energy bins (as GeV) as indicated.

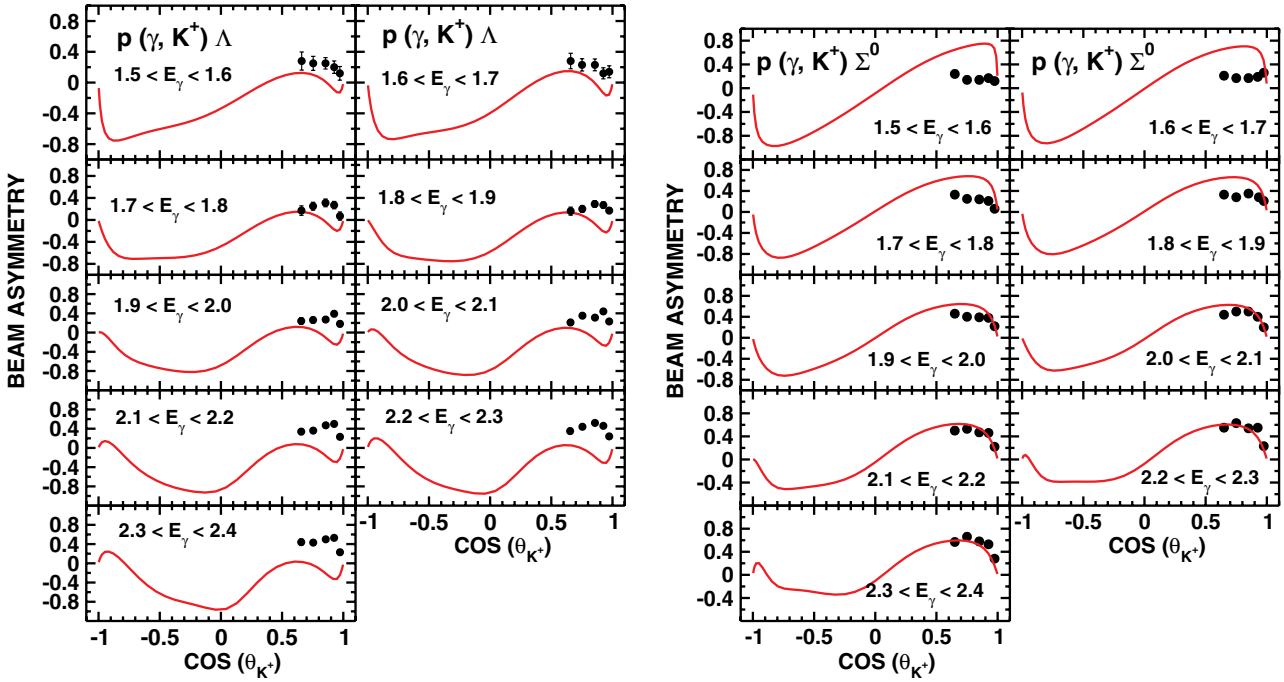

FIG. 12. (Color online) Beam asymmetry for the $p(\gamma,K^+)\Lambda$ and $p(\gamma,K^+)\Sigma^0$ reactions as a function of the cosine of the K^+ c.m. angle for 15 photon energies. Experimental data are taken from Ref. [5].

and $p(\gamma,K^+)\Sigma^0$ reactions with the corresponding data taken from Refs. [5] and [6], which are available for nine energy bins for photon energies between 1.5 and 2.3 GeV. Available experimental Σ_B values are positive for both reactions. Our calculations reproduce the data with varying degrees of success. For the $p(\gamma,K^+)\Lambda$ reaction the agreement with the data is relatively better for $E_\gamma < 2.0$ GeV. For larger E_γ the data are underestimated by our model. On the other hand, for the $p(\gamma,K^+)\Sigma^0$ case the data are described better for $E_\gamma >$ 1.9 GeV, whereas at lower photon energies they are overestimated. In calculations reported in Ref. [26] a comparison with the data is shown for the $K^+\Lambda$ channel for one photon energy ($E_\gamma = 1.946$ GeV) only. In the coupled-channels analysis in Ref. [34], the agreement with the Σ_B data for the $p(\gamma,K^+)\Lambda$ reactions is of the same quality as that we achieved: there too the data are better reproduced for $E_\gamma < 2.0$ GeV, whereas they are underpredicted at energies higher than this. However, we emphasize that such data for both $K^+\Lambda$ and $K^+\Sigma^0$ channels have not been analyzed simultaneously with one parameter set in any other coupled-channels model.

IV. SUMMARY AND CONCLUSIONS

In this paper we have investigated the photoproduction reactions $p(\gamma,K^+)\Lambda$ and $p(\gamma,K^+)\Sigma^0$ within a coupled-channels effective-Lagrangian approach that is based on the K-matrix method. Unitarity effects are correctly taken into account, because all important final channels (consisting of two-body systems πN, ηN, ϕN, ρN, γN, $K\Lambda$, and $K\Sigma$) are included in the K-matrix kernel. We build this kernel by using effective Lagrangians for the Born, u-channel, t-channel, and spin-$\frac{1}{2}$ and spin-$\frac{3}{2}$ resonance contributions. Thus, the background contributions are generated consistently and crossing symmetry is obeyed. The advantage of a full coupled-channels calculation is that it allows for the simultaneous calculation of observables for a large multitude of reactions with considerably fewer parameters than would be necessary if each reaction channel were fitted separately. More significantly, the implementation of unitarity ensures that the imaginary parts of the amplitudes are compatible with the cross sections for other channels.

Our model provides a reasonable description of the experimental data of the SAPHIR group on total cross sections and DCSs as well as on hyperon polarizations for photon energies ranging from threshold up to ≈3 GeV for both $p(\gamma,K^+)\Lambda$ and $p(\gamma,K^+)\Sigma^0$ reactions. The beam asymmetry data from the SPring8/LEPS group for the two reactions are also reasonably reproduced.

An important point regarding our study is that the same parameter set was used in calculating observables for both the reactions.

We made a detailed investigation of the contribution of various partial waves and showed that peaks seen in the total $p(\gamma,K^+)\Lambda$ cross sections for photon energies around 1.5 GeV (invariant mass of 1.9 GeV) are largely caused by coupled-channels effects rather than the contribution of a D-wave resonance with a mass around 1.9 GeV. A major part of the cross sections of this reaction is generated via the background terms, and resonances make prominent contributions only in the first peak region (for E_γ around 1.1 GeV). On the other hand, the total $p(\gamma,K^+)\Sigma^0$ cross sections are dominated by the $P_{33}(1600)$ resonance in its peak region (E_γ around 1.5 GeV).

The agreement between our calculations and the DCS data of the CLAS Collaboration is not of the same quality as that seen in the case of the SAPHIR data, particularly at extreme forward angles. At some backward angles the CLAS data show pronounced peaks for some photon energies, but no peak is seen in the corresponding SAPHIR data or in our theoretical cross sections. Whether or not these peaks are an indication for an additional P- or D-wave resonance is a matter of debate and for additional investigations. In this context, it is quite desirable to settle the issue of mutual inconsistency between the CLAS and the SAPHIR data sets.

Our work shows that it is indeed possible to fit meson photoproduction data for many channels simultaneously with a single parameter set within a coupled-channels model. Further improvement of our model is necessary, however, for a better description of the data at extreme forward angles in the case of higher photon energies.

ACKNOWLEDGMENTS

This work was supported by Sonderforschungsbereich/ Transregio 16, Bonn–Giessen–Bochum, of the German Research Foundation (DFG) and the Dutch Organization for Scientific Research (NWO).

APPENDIX: EFFECTIVE LAGRANGIANS

We list here the effective Lagrangians for various vertices. p, k, p', and $-q$ represent four momenta of the initial nucleon, final meson, final nucleon, and photon, respectively. We assume that meson momenta are directed into the vertex, so that energy momentum conservation reads as $p + k = p' - q$.

For the nucleon vertices the following couplings were used:

$$
\begin{aligned}
\mathcal{L}_{NN\pi} &= i g_{NN\pi} \bar{\Psi}_N \frac{(\chi \boldsymbol{\varphi}_\pi + i \partial \boldsymbol{\varphi}_\pi / 2m_N) \cdot \boldsymbol{\tau}}{\chi + 1} \gamma_5 \Psi_N, \\
\mathcal{L}_{NN\eta} &= i g_{NN\eta} \bar{\Psi}_N \frac{\chi \varphi_\eta + i \partial \varphi_\eta / 2m_N}{\chi + 1} \gamma_5 \Psi_N, \\
\mathcal{L}_{NN\sigma} &= -g_{NN\sigma} \bar{\Psi}_N \varphi_\sigma \Psi_N, \\
\mathcal{L}_{NN\rho} &= -g_{NN\rho} \bar{\Psi}_N \left(\gamma_\mu \boldsymbol{\varphi}^\mu_\rho + \frac{\kappa_\rho}{2m_N} \sigma_{\mu\nu} \partial^\nu \boldsymbol{\varphi}^\mu_\rho \right) \cdot \boldsymbol{\tau} \Psi_N, \\
\mathcal{L}_{NN\omega} &= -g_{NN\omega} \bar{\Psi}_N \left(\gamma_\mu \varphi^\mu_\omega + \frac{\kappa_\omega}{2m_N} \sigma_{\mu\nu} \partial^\nu \varphi^\mu_\omega \right) \Psi_N, \\
\mathcal{L}_{NN\phi} &= -g_{NN\phi} \bar{\Psi}_N \left(\gamma_\mu \varphi^\mu_\phi + \frac{\kappa_\phi}{2m_N} \sigma_{\mu\nu} \partial^\nu \varphi^\mu_\phi \right) \Psi_N, \\
\mathcal{L}_{NN\gamma} &= -e \bar{\Psi}_N \left(\frac{1 + \tau_0}{2} \gamma_\mu A^\mu + \frac{\kappa_\tau}{2m_N} \sigma_{\mu\nu} \partial^\nu A^\mu \right) \Psi_N, \\
\mathcal{L}_{NN\gamma\varphi} &= -e \frac{g_{NN\phi}}{2m_N} \bar{\Psi}_N \gamma_5 \gamma_\mu [\boldsymbol{\tau} \times \boldsymbol{\varphi}] A^\mu. \qquad \text{(A1)}
\end{aligned}
$$

The parameter χ controls the admixture of pseudoscalar and pseudovector components in the corresponding Lagrangian. Its value is taken to be 0.5. This value was obtained in our previous study of photoproduction of associated strangeness [25] and has been held fixed in the study of all other reactions within our model. Nucleon spinors are denoted Ψ, and meson fields by φ. The magnetic moments are represented by κ. $\mathcal{L}_{NN\gamma\varphi}$ generates the seagull or the contact-term diagrams. We have followed the notations of Ref. [64].

The Lagrangians for the meson vertices are

$$
\begin{aligned}
\mathcal{L}_{\rho\pi\pi} &= -g_{\rho\pi\pi} \boldsymbol{\varphi}_{\rho_\mu} \cdot (\boldsymbol{\varphi}_\pi \times \overleftrightarrow{\partial^\mu} \boldsymbol{\varphi}_\pi)/2, \\
\mathcal{L}_{\gamma\pi\pi} &= e \varepsilon_{3ij} A_\mu (\varphi_{\pi_i} \overleftrightarrow{\partial^\mu} \varphi_{\pi j}), \\
\mathcal{L}_{\rho\gamma\pi} &= e \frac{g_{\rho\gamma\pi}}{m_\pi} \boldsymbol{\varphi}_\pi \cdot \left[\varepsilon_{\mu\nu\rho\sigma} (\partial^\rho A^\mu) \left(\partial^\sigma \boldsymbol{\varphi}^\nu_\rho \right) \right], \\
\mathcal{L}_{\omega\gamma\pi} &= e \frac{g_{\omega\gamma\pi}}{m_\pi} \varphi_{\pi^0} [\varepsilon_{\mu\nu\rho\sigma} (\partial^\rho A^\mu) (\partial^\sigma \omega^\nu)], \\
\mathcal{L}_{\phi\gamma\pi} &= e \frac{g_{\phi\gamma\pi}}{m_\pi} \boldsymbol{\varphi}_{\pi^0} [\varepsilon_{\mu\nu\rho\sigma} (\partial^\rho A^\mu) (\partial^\sigma \phi^\nu)], \\
\mathcal{L}_{\phi\gamma\eta} &= e \frac{g_{\phi\gamma\eta}}{m_\pi} \varphi_\eta \left[\varepsilon_{\mu\nu\rho\sigma} (\partial^\rho A^\mu) \left(\partial^\sigma \varphi^\nu_\phi \right) \right], \\
\mathcal{L}_{\rho\gamma\eta} &= e \frac{g_{\rho\gamma\eta}}{m_\pi} \varphi_\eta \left[\varepsilon_{\mu\nu\rho\sigma} (\partial^\rho A^\mu) \left(\partial^\sigma \varphi_{\rho^0}{}^\nu \right) \right], \\
\mathcal{L}_{\rho\gamma\sigma} &= e \frac{g_{\rho\gamma\sigma}}{m_\rho} (\partial^\mu \varphi_{\rho^\nu} \partial_\mu A_\nu - \partial^\mu \varphi_{\rho^\nu} \partial_\nu A_\mu), \\
\mathcal{L}_{\rho\rho\gamma} &= 2e \big[A^\mu (\partial_\mu \varphi_{\rho_\nu}) \tau_0 \varphi_\rho{}^\nu - (\partial^\nu A^\mu) \varphi_{\rho_\nu} \tau_0 \varphi_{\rho_\mu} \\
&\quad + (\partial^\nu A^\mu) \varphi_{\rho_\mu} \tau_0 \varphi_{\rho_\nu} \big], \\
\mathcal{L}_{\phi KK} &= -i g_{\phi KK} \bar{\boldsymbol{\varphi}}_K (\overleftrightarrow{\partial^\mu} \boldsymbol{\varphi}_K) \phi_\mu, \\
\mathcal{L}_{\eta K^* K} &= -i g_{\eta K K^*} \boldsymbol{\varphi}_K \overleftrightarrow{\partial^\mu} \varphi_\eta \bar{\boldsymbol{\varphi}}_{K^* \mu}, \\
\mathcal{L}_{\pi K^* K} &= -i g_{\pi K K^*} \bar{\boldsymbol{\varphi}}_K \overleftrightarrow{\partial^\mu} \boldsymbol{\varphi}_\pi \cdot \boldsymbol{\tau} \boldsymbol{\varphi}_{K^* \mu}, \\
\mathcal{L}_{\rho\pi\eta} &= -i g_{\rho\pi\eta} (\varphi_\eta \overleftrightarrow{\partial^\mu} \boldsymbol{\varphi}_\pi) \boldsymbol{\varphi}_{\rho_\mu}, \\
\mathcal{L}_{K^* K^0 \gamma} &= \frac{g_{K^* K \gamma}}{m_\pi} \bar{\boldsymbol{\varphi}}_{K^0} \left[\varepsilon_{\mu\nu\rho\sigma} (\partial^\rho A^\mu) \left(\partial^\sigma \boldsymbol{\varphi}^\nu_{K^*} \right) \right], \\
\mathcal{L}_{K^* K^\pm \gamma} &= \frac{g_{K^* K \gamma}}{m_\pi} \bar{\boldsymbol{\varphi}}_{K^\pm} \left[\varepsilon_{\mu\nu\rho\sigma} (\partial^\rho A^\mu) \left(\partial^\sigma \boldsymbol{\varphi}^\nu_{K^*} \right) \right]. \qquad \text{(A2)}
\end{aligned}
$$

The coupling constants entering into Eqs. (A1) and (A2) together with the baryon magnetic moments are listed in Table III. We have taken positive values for all primary

TABLE III. Parameter summary table.

$g_{NN\pi}$	13.47	$g_{NN\eta}$	0.85
$g_{NN\sigma}$	10.0	$g_{NN\rho}$	4.2
$g_{NN\omega}$	3.0	$g_{NN\phi}$	−0.0
$g_{\Sigma\sigma\rho}$	33.0	$g_{\Sigma\Lambda\rho}$	−27.0
$g_{\rho\pi\pi}$	6.0	$g_{\rho\pi\eta}$	0.0
$g_{\rho\pi^0\gamma}$	−0.12	$g_{\rho\pi^\pm\gamma}$	−0.10
$g_{\rho\eta\gamma}$	−0.21	$g_{\omega\eta\gamma}$	−0.12
$g_{\omega\pi\gamma}$	0.32	$g_{\rho\sigma\gamma}$	12.0
$g_{N\Lambda K}$	10.0	$g_{N\Sigma K}$	14.5
$g_{N\Lambda K^*}$	−3.3	$g_{N\Sigma K^*}$	0.0
$g_{\phi KK}$	−4.5	$g_{\rho KK}$	−3.0
$g_{\pi KK^*}$	−3.26	$g_{\eta KK^*}$	−3.2
$g_{K^*K^0\gamma}$	0.177	$g_{K^*K^\pm\gamma}$	−0.177
κ_p	1.79	κ_n	−1.91
κ_Λ	−0.613	κ_{Σ^0}	0.79
κ_{Σ^+}	1.45	κ_{Σ^-}	−0.16
$\kappa_{\Sigma^0\to\Lambda\gamma}$	−1.61		

coupling constants involving the nucleon. In particular, the sign of $g_{NK\Lambda}$ differs from its customary negative value [65] However, we would like to stress that in a calculation like ours, and also in many of those cited in Ref. [65], this sign is undetermined. Changing the sign of all the coupling constants involving a single Λ field leaves the calculated observables invariant, as it corresponds to a sign redefinition of this field. The magnitudes of the couplings are within the broad range specified in Ref. [65].

For the S_{11}, S_{31}, P_{11}, and P_{31} resonances the hadronic couplings are written as

$$\mathcal{L}_{\varphi N R_{1/2}} = -g_{\varphi N R}\bar{\Psi}_R\left[\chi i\Gamma\varphi + (1-\chi)\frac{1}{M}\Gamma\gamma_\mu(\partial^\mu\varphi)\right] \times \Psi_N + \text{H.c.}, \tag{A3}$$

where $M = (m_R \pm m_N)$, with upper sign for even-parity and lower sign for odd-parity resonance. The operator Γ is γ_5 and unity for even- and odd-parity resonances, respectively. For isovector mesons, φ in Eq. (A3) needs to be replaced with $\boldsymbol{\tau}\cdot\boldsymbol{\varphi}$ for isospin-$\frac{1}{2}$ resonances and with $\mathbf{T}\cdot\boldsymbol{\varphi}$ otherwise.

The corresponding electromagnetic couplings are

$$\mathcal{L}_{\gamma N R_{1/2}} = -eg_1\bar{\Psi}_R\frac{\Gamma}{4m_N}\sigma_{\mu\nu}\Psi_N F^{\mu\nu} + \text{H.c.}, \tag{A4}$$

where Ψ_R is the resonance spinor and $F^{\mu\nu} = \partial^\mu A^\nu - \partial^\nu \mathsf{A}^\mu$. The operator Γ is 1 for the positive-parity resonance and $-i\gamma_5$ for the negative-parity one.

For spin-$\frac{3}{2}$ resonances, we have used the gauge-invariant effective Lagrangians as discussed in Refs. [50], [57], [58], [66], and [67]. We write here the vertex functions that we used in computation involving these vertices. The resonance-nucleon-pion vertex function (e.g.) is given by

$$\Gamma^\alpha_{R_{3/2}\to N\pi} = \frac{g_1}{m_\pi}[\gamma^\alpha(q\cdot p) - \not{p}q^\alpha][(1-\chi) + \chi\not{p}/M_p], \tag{A5}$$

and the corresponding electromagnetic vertices are

$$\begin{aligned}\Gamma^{\alpha\mu}_{R_{3/2}\to N\gamma} = \{&(g_2+2g_1)[q^\alpha p^\mu - g^{\alpha\mu}p\cdot q] \\ &+ g_1[g^{\alpha\mu}\not{p}\not{q} - q^\alpha\not{p}\gamma^\mu + \gamma^\alpha(\gamma^\mu p\cdot q - p^\mu\not{q})] \\ &+ g_3[(-q^2 g^{\alpha\mu} + q^\mu q^\alpha)\not{p} \\ &+ (q^2 p^\mu - q^\mu p\cdot q)\gamma^\alpha]\}\gamma_5[(1-\chi) + \chi\not{p}/M_p].\end{aligned} \tag{A6}$$

Here p is the four-momentum of the resonance and q is that of the meson. Index α belongs to the spin-$\frac{3}{2}$ spinor and μ to the photon. An interesting property of these vertices is that the product $p\cdot\Gamma = 0$, where Γ defines the vertices on the left-hand side of Eqs. (A5) and (A6). As a consequence, the spin-$\frac{1}{2}$ part of the corresponding propagator becomes redundant, as its every term is proportional to either p_μ or p_ν. Thus only the spin-$\frac{3}{2}$ part of this propagator gives rise to nonvanishing matrix elements.

[1] R. Bradford *et al.*, Phys. Rev. C **73**, 035202 (2006); R. A. Schumacher (private communication, 2009).
[2] J. W. C. McNabb *et al.*, Phys. Rev. C **69**, 042201 (2004).
[3] K. H. Glander *et al.*, Eur. Phys. J. A **19**, 251 (2004).
[4] R. Lawall *et al.*, Eur. Phys. J. A **24**, 275 (2005).
[5] R. G. T. Zengers *et al.*, Phys. Rev. Lett. **91**, 092001 (2003).
[6] M. Sumihama *et al.*, Phys. Rev. C **73**, 035214 (2006).
[7] R. Bradford *et al.*, Phys. Rev. C **75**, 035205 (2007).
[8] S. Capstick and W. Roberts, Prog. Part. Nucl. Phys. **45**, S241 (2000), and references therein.
[9] A. Walker-Loud, H.-W. Lin, D. G. Richards, R. G. Edwards, M. Engelhardt, G. T. Fleming, Ph. Hagler, B. Musch, M. F. Lin, H. B. Meyer, J. W. Negele, A. V. Pochinsky, M. Procura, S. Syritsyn, C. J. Morningstar, K. Orginos, D. B. Renner, and W. Schroers, Phys. Rev. D **79**, 054502 (2009).
[10] S. Basak, R. G. Edwards, G. T. Fleming, K. J. Juge, A. Lichtl, C. Morningstar, D. G. Richards, I. Sato, and S. J. Wallace, Phys. Rev. D **76**, 074504 (2007).
[11] T. Burch, C. Gattringer, L. Ya. Glozman, C. Hagen, D. Hierl, C. B. Lang, and A. Schäfer, Phys. Rev. D **74**, 014504 (2006).
[12] N. Mathur, Y. Chen, S. J. Dong, T. Draper, I. Horváth, F. X. Lee, K. F. Liu, and J. B. Zhang, Phys. Lett. **B605**, 137 (2005).
[13] D. B. Leinweber, W. Melnitchouk, D. G. Richards, A. G. Williams, and L. M. Zanotti, in *Lattice Hadron Physics*, edited by A. Kalloniatis, D. Leinweber, and A. Williams (Springer, Berlin, 2005), p. 71; J. M. Zanotti, B. Lasscock, D. B. Leinweber, and A. G. Williams, Phys. Rev. D **71**, 034510 (2005); R. D. Young, D. B. Leinweber, and A. W. Thomas, *ibid.* **71**, 014001 (2005).
[14] U. Löring, K. Kretzschmar, B. C. Metsch, and H. R. Petry, Eur. Phys. J. A **10**, 395 (2001).
[15] M. F. M. Lutz and E. E. Kolomeitsev, Nucl. Phys. **A755**, 29 (2005); J. Hofmann and M. F. M. Lutz, *ibid.* **A763**, 90 (2005); **A776**, 17 (2006).
[16] M. Benmerrouche, N. C. Mukhopadhyay, and J. F. Zhang, Phys. Rev. D **51**, 3237 (1995); N. C. Mukhopadhyay and N. Mathur, Phys. Lett. **B444**, 7 (1998); R. M. Davidson, N. Mathur, and N. C. Mukhopadhyay, Phys. Rev. C **62**, 058201 (2000).
[17] R. Workman, R. A. Arndt, and I. I. Strakovsky, Phys. Rev. C **62**, 048201 (2000); R. A. Arndt, W. J. Briscoe, I. I. Strakovsky, and R. L. Workman, *ibid.* **66**, 055213 (2002); Ya. I. Azimov, R. A. Arndt, I. I. Strakovsky, and R. L. Workman, *ibid.* **68**, 045204 (2003); R. A. Arndt, W. J. Briscoe, I. I. Strakovsky, and R. L. Workman, *ibid.* **72**, 058203 (2005).
[18] L. Tiator, D. Drechsel, G. Knöchlein, and C. Bennhold, Phys. Rev. C **60**, 035210 (1999).
[19] D. Drechsel, O. Hanstein, S. S. Kamalov, and L. Tiator, Nucl. Phys. **A645**, 145 (1999).
[20] R. Shyam, Phys. Rev. C **75**, 055201 (2007); **60**, 055213 (1999); R. Shyam, G. Penner, and U. Mosel, *ibid.* **63**, 022202(R) (2001); R. Shyam, *ibid.* **73**, 035211 (2006).
[21] S. Janssen, J. Ryckebusch, D. Debruyne, and T. Van Cauteren, Phys. Rev. C **65**, 015201 (2001).
[22] T. Feuster and U. Mosel, Phys. Rev. C **58**, 457 (1998); **59**, 460 (1999).
[23] A. Yu. Korchin, O. Scholten, and R. G. E. Timmermans, Phys. Lett. **B438**, 1 (1998).
[24] G. Penner and U. Mosel, Phys. Rev. C **66**, 055211 (2002); **66**, 055212 (2002); G. Penner, Ph.D. thesis, Universität Giessen, 2002 (in English; available at http://theorie.physik.uni-giessen.de).

[25] A. Usov and O. Scholten, Phys. Rev. C **72**, 025205 (2005).
[26] V. Shklyar, H. Lenske, and U. Mosel, Phys. Rev. C **72**, 015210 (2005).
[27] A. Usov and O. Scholten, Phys. Rev. C **74**, 015205 (2006).
[28] R. Shyam and O. Scholten, Phys. Rev. C **78**, 065201 (2008).
[29] J. Durand, B. Julia-Diaz, T.-S. H. Lee, B. Saghai, and T. Sato, Phys. Rev. C **78**, 025204 (2008).
[30] B. Julia-Diaz, T.-S. H. Lee, A. Matsuyama, T. Sato, and L. C. Smith, Phys. Rev. C **77**, 045205 (2008).
[31] B. Julia-Diaz, T.-S. H. Lee, A. Matsuyama, and T. Sato, Phys. Rev. C **76**, 065201 (2007).
[32] B. Saghai, J.-C. David, B. Julia-Diaz, and T.-S. H. Lee, Eur. Phys. J. A **31**, 512 (2007).
[33] B. Julia-Diaz, B. Saghai, F. Tabakin, W.-T. Chiang, T.-S. H. Lee, and Z. Li, Nucl. Phys. **A755**, 463c (2005).
[34] B. Julia-Diaz, B. Saghai, T.-S. H. Lee, and F. Tabakin, Phys. Rev. C **73**, 055204 (2006).
[35] W.-T. Chiang, F. Tabakin, T.-S. H. Lee, and B. Saghai, Phys. Lett. **B517**, 101 (2001).
[36] T. Mart, C. Bennhold, H. Haberzettl, and L. Tiator (http://www.kph.uni-mainz.de/kaonmaid.html).
[37] J. C. David, C. Fayard, G.-H. Lamot, and B. Saghai, Phys. Rev. C **53**, 2613 (1996).
[38] T. Mart and C. Bennhold, Phys. Rev. C **61**, 012201(R) (1999).
[39] T. Mart and A. Sulaksono, Phys. Rev. C **74**, 055203 (2006); P. Bydzovsky and T. Mart, *ibid*. **76**, 065202 (2007).
[40] R. A. Adelseck, C. Bennhold, and L. E. Wright, Phys. Rev. C **32**, 1681 (1985).
[41] R. A. Adelseck, and B. Saghai, Phys. Rev. C **42**, 108 (1990).
[42] R. A. Williams, C. R. Ji, and S. R. Cotanch, Phys. Rev. C **43**, 452 (1991).
[43] B. S. Han, M. K. Cheoun, K. S. Kim, and I. T. Cheon, Nucl. Phys. **A691**, 713 (2001).
[44] Z. Li, Phys. Rev. C **52**, 1648 (1995).
[45] D. Lu, R. H. Landau, and S. C. Phatak, Phys. Rev. C **52**, 1662 (1995).
[46] J. He, B. Saghai, and Z. Li, Phys. Rev. C **78**, 035204 (2008).
[47] B. Borasoy, P. C. Bruns, U.-G. Meissner, and R. Nissler, Eur. Phys. J. A **34**, 161 (2007).
[48] O. Scholten, S. Kondratyuk, L. Van Daele, D. Van Neck, M. Waroquier, and A. Yu. Korchin, Acta Phys. Pol. B **33**, 847 (2002).
[49] R. G. Newton, *Scattering Theory of Waves and Particles* (Springer, New York, 1982).
[50] S. Kondratyuk and O. Scholten, Nucl. Phys. **A677**, 396 (2000); Phys. Rev. C **62**, 025203 (2000).
[51] S. Kondratyuk and O. Scholten, Phys. Rev. C **65**, 038201 (2002); **64**, 024005 (2001).
[52] A. Yu. Korchin and O. Scholten, Phys. Rev. C **68**, 045206 (2003).
[53] T. Sato and T.-S. H. Lee, Phys. Rev. C **54**, 2660 (1996).
[54] W. T. Chiang, B. Saghai, F. Tabakin, and T.-S. H. Lee, Phys. Rev. C **69**, 065208 (2004).
[55] M. F. M. Lutz and E. E. Kolomeitsev, Nucl. Phys. **A700**, 193 (2002).
[56] S. Kondratyuk, K. Kubodera, F. Myhrer, and O. Scholten, Nucl. Phys. **A736**, 339 (2004).
[57] V. Pascalutsa, Nucl. Phys. **A680**, 76 (2000).
[58] V. Pascalutsa, Phys. Lett. **B503**, 85 (2001).
[59] W. M. Yao *et al.* (Particle Data Group), J. Phys. G **33**, 1 (2006).
[60] R. M. Davidson and R. Workman, Phys. Rev. C **63**, 025210 (2001).
[61] Virginia Tech SAID database, http://gwdac.phys.hwu.edu/, FA08 solution; R. A. Arndt, I. I. Strakovsky, and R. L. Workman, Phys. Rev. C **53**, 430 (1996); R. A. Arndt, W. J. Briscoe, I. I. Strakovsky, and R. L. Workman, *ibid*. **74**, 045205 (2006).
[62] N. Kaiser, T. Waas, and W. Weise, Nucl. Phys. **A612**, 297 (1997).
[63] A. V. Sarantsev, V. A. Nikonov, A. V. Anisovich, E. Klempt, and U. Thoma, Eur. Phys. J. A **25**, 441 (2005).
[64] J. D. Bjorken and S. D. Drell, *Relativistic Quantum Mechanics* (McGraw–Hill, New York, 1964).
[65] I. J. General and S. R. Cotanch, Phys. Rev. C **69**, 035202 (2004).
[66] V. Pascalutsa, Phys. Rev. D **58**, 096002 (1998).
[67] L. Jahnke and S. Leupold, Nucl. Phys. **A778**, 53 (2006).